Snow Loss into Leads in Arctic Sea Ice: Minimal in Typical Wintertime Conditions, but High During a Warm and Windy Snowfall Event

David Clemens-Sewall[1], Chris M Polashenski[2], Markus Michael Frey[3], Christopher J. Cox[4], Mats Anders Granskog[5], Amy Macfarlane[6], Steven Fons[7], Julia Schmale[8], Jennifer Katy Hutchings[9], Luisa von Albedyll[10], Stefanie Arndt[11], Martin Schneebeli[6], and Donald Perovich[12]

[1]Thayer School of Engineering at Dartmouth College
[2]USACE-CRREL/Dartmouth College
[3]British Antarctic Survey
[4]CIRES/NOAA-ESRL
[5]Norwegian Polar Institute
[6]WSL Institute for Snow and Avalanche Research SLF
[7]University of Maryland - College Park
[8]École Polytechnique Fédérale de Lausanne
[9]Oregon State University
[10]Alfred Wegener Institute, Helmholtz Centre for Polar and Marine Research
[11]Alfred-Wegener-Institut Helmholtz-Zentrum für Polar- und Meeresforschung
[12]Dartmouth College

February 27, 2023

Abstract

The amount of snow on Arctic sea ice impacts the ice mass budget. Wind redistribution of snow into open water in leads is hypothesized to cause significant wintertime snow loss. However, there are no direct measurements of snow loss into Arctic leads. We measured the snow lost in four leads in the Central Arctic in winter 2020. We find, contrary to the general consensus, that under typical winter conditions, minimal snow was lost into leads. However, during a cyclone that delivered warm air temperatures, high winds, and snowfall, 35.0 $\pm$ 1.1 cm snow water equivalent (SWE) was lost into a lead (per unit lead area). This corresponded to a removal of 0.7–1.1 cm SWE from the entire surface— 6–10% of this site's annual snow precipitation. Warm air temperatures, which increase the length of time that wintertime leads remain unfrozen, may be an underappreciated factor in snow loss into leads.

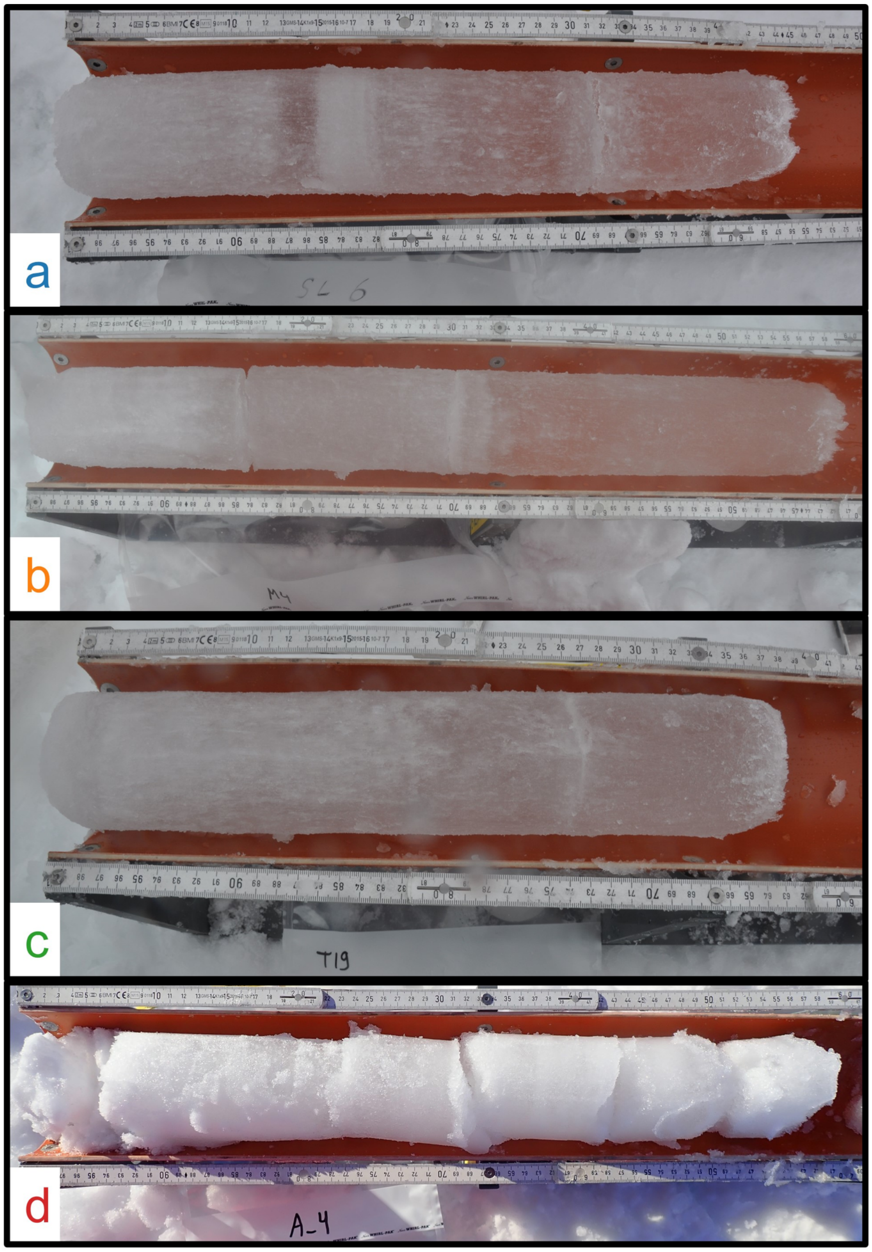
a
SL 6
b
M4
c
T19
d
A_4

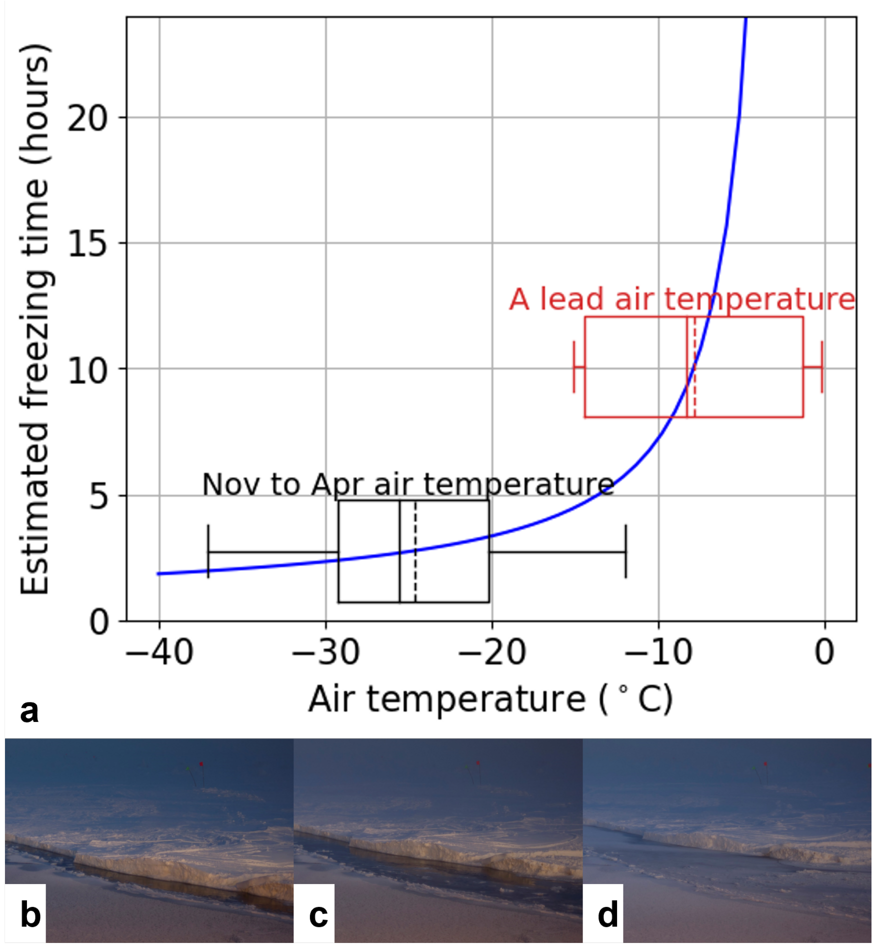

Estimated freezing time (hours)
0
5
10
15
20
A lead air temperature
Nov to Apr air temperature
−40
−30
−20
−10
0
Air temperature (∘ C)
a
b
c
d

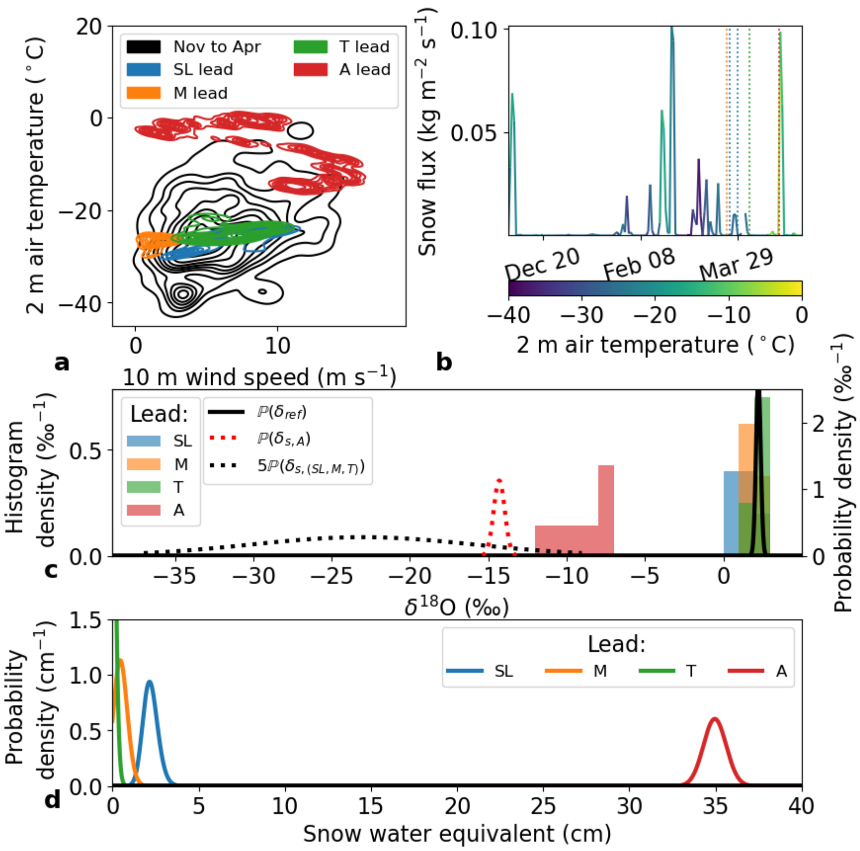

a
2 m air temperature (°C)
10 m wind speed (m s^{-1})
Nov to Apr
SL lead
M lead
T lead
A lead
b
Snow flux (kg m^{-2} s^{-1})
Dec 20
Feb 08
Mar 29
2 m air temperature (°C)
c
Histogram density (‰$^{-1}$)
Probability density (‰$^{-1}$)
Lead:
SL
M
T
A
$\mathbb{P}(\delta_{ref})$
$\mathbb{P}(\delta_{s,A})$
$5\mathbb{P}(\delta_{s,(SL,M,T)})$
δ^{18}O (‰)
d
Probability density (cm^{-1})
Lead:
SL
M
T
A
Snow water equivalent (cm)

Snow Loss into Leads in Arctic Sea Ice: Minimal in Typical Wintertime Conditions, but High During a Warm and Windy Snowfall Event

David Clemens-Sewall[1], Chris Polashenski[1,2], Markus M. Frey[3], Christopher J. Cox[4], Mats A. Granskog[5], Amy R. Macfarlane[6], Steven W. Fons[7,8], Julia Schmale[9], Jennifer K. Hutchings[10], Luisa von Albedyll[11], Stefanie Arndt[11], Martin Schneebeli[6], Don Perovich[1]

[1]Thayer School of Engineering, Dartmouth College, Hanover, NH, USA
[2]Cold Regions Research and Engineering Laboratory, US Army Corps of Engineers, Hanover, NH, USA
[3]British Antarctic Survey – Natural Environment Research Council, Cambridge, UK
[4]NOAA Physical Sciences Laboratory, Boulder, CO, USA
[5]Norwegian Polar Institute, Fram Centre, Tromsø, Norway
[6]WSL Institute for Snow and Avalanche Research SLF, Davos, Switzerland
[7]Cryospheric Sciences Laboratory, NASA Goddard Space Flight Center, Greenbelt, MD, USA
[8]Earth System Science Interdisciplinary Center, University of Maryland, College Park, MD, USA
[9]Extreme Environments Research Laboratory, École Polytechnique Fédérale de Lausanne, Sion, Switzerland
[10]College of Earth, Ocean, and Atmospheric Sciences, Oregon State University, Corvallis, OR, USA
[11]Alfred-Wegener-Institut, Helmholtz-Zentrum für Polar- und Meeresforschung, Bremerhaven, Germany

Key Points:

- Minimal snow was lost into leads in observations of three cases in typical wintertime, cold, moderately windy conditions on Arctic sea ice.
- In an atmospheric advection event with air temperature above -10 C, high wind, and fresh snowfall, most recent snowfall was lost into leads.
- Warm air temperatures increase the duration of unfrozen water in leads, which may be an underappreciated factor in snow loss into leads.

Corresponding author: David Clemens-Sewall, `David.W.Clemens-Sewall.Th@dartmouth.edu`

Abstract

The amount of snow on Arctic sea ice impacts the ice mass budget. Wind redistribution of snow into open water in leads is hypothesized to cause significant wintertime snow loss. However, there are no direct measurements of snow loss into Arctic leads. We measured the snow lost in four leads in the Central Arctic in winter 2020. We find, contrary to the general consensus, that under typical winter conditions, minimal snow was lost into leads. However, during a cyclone that delivered warm air temperatures, high winds, and snowfall, 35.0 $\pm$ 1.1 cm snow water equivalent (SWE) was lost into a lead (per unit lead area). This corresponded to a removal of 0.7–1.1 cm SWE from the entire surface—$\sim$6–10% of this site's annual snow precipitation. Warm air temperatures, which increase the length of time that wintertime leads remain unfrozen, may be an underappreciated factor in snow loss into leads.

Plain Language Summary

The amount of snow on Arctic sea ice impacts how quickly the ice grows in the winter and melts in the summer. Cracks in the ice, known as leads, expose ocean water that snow can be blown into, reducing the amount of snow on the ice and thus impacting ice growth and melt. We found that in typical wintertime conditions, very little snow is blown into leads. However, if there is fresh snowfall, it is uncommonly warm and it is very windy at the same time when leads are forming, a large amount of snow can be blown into the ocean. Accounting for the impacts of air temperature on this process will enable scientists to better understand how much snow is on Arctic sea ice, and hence how quickly the ice grows in the winter and melts in the summer, and how this might change in a future, warmer, Arctic.

1 Introduction

Snow on Arctic sea ice impacts the energy budget and mass balance of the ice. The insulating properties of snow limit ice growth in the winter (Maykut & Untersteiner, 1971; Sturm et al., 2002) whereas its high albedo (Warren, 2019) slows ice melt in the summer (Perovich et al., 2002; Perovich & Polashenski, 2012). Snow on sea ice is a freshwater source for melt ponds (Polashenski et al., 2012) and habitat for biota (Iacozza & Ferguson, 2014). Despite this importance, the snow mass balance on Arctic sea ice remains uncertain. Several poorly-constrained processes contribute to the net budget, including: precipitation, deposition, sublimation, melting, flooding (snow-ice formation), superimposed ice formation, and wind-blown snow redistribution into open water leads (snow loss into leads).

Snow loss into leads has been estimated to consume up to 50% of the snowfall on Antarctic sea ice (Leonard & Maksym, 2011). The applicability of these estimates to the Arctic is unclear. There are no published direct measurements of snow loss into leads in the Arctic. Nevertheless, parameterizations of the process have been developed and implemented in climate models (Lecomte et al., 2015) and data assimilation products (Petty et al., 2018). For example, Petty et al. (2018) modelled that blowing snow loss into leads reduced the snow depth on sea ice North of 60°N by 10 cm throughout the winter (approximately a 25% reduction).

Here, we present the first measurements of snow loss into Arctic leads from four cases we observed in detail in winter 2020 in the Atlantic sector of the Central Arctic Ocean. Snow loss into leads was determined from the δ^{18}O of the lead ice, a signature routinely used to identify snow contributions to sea ice (Jeffries et al., 1994, 1997, 2001; Kawamura et al., 2001; Granskog et al., 2003, 2004, 2017; Tian et al., 2020; Arndt et al., 2021). When snow enters seawater in a lead, the snow is less dense than seawater and consequently floats at the surface. If there is sufficient heat at the ocean surface to melt the snow, the resulting freshwater is less dense than seawater. As the lead freezes, the snow (solid or melted) is incorporated into the lead ice. Due to isotopic fractionation, snow is depleted in ^{18}O relative to seawater (Dansgaard, 1953). We contextualize the observations with atmospheric conditions at the time of lead formation to infer controls that may limit or promote snow loss into leads.

2 Materials and Methods

2.1 Overview of data collection

During the Multidisciplinary drifting Observatory for the Study of Arctic Climate (MOSAiC) expedition, R/V Polarstern drifted with the same assembly of sea ice floes in the Arctic Ocean from October 2019 to May 2020 (Nicolaus et al., 2022; Shupe et al., 2022; Rabe et al., 2022). In March and April 2020 within 1 km of Polarstern, we observed the formation of approximately 18 leads ranging in width from 5 m to greater than 100 m. Whenever possible, we identified the timing of lead formation and refreezing to within

20 minutes by visual observations and time-lapse panoramic imagery from a camera mounted on Polarstern's crow's nest (Nicolaus et al., 2021). Near-surface meteorology and localized snow depth were measured continuously from a tower and two mobile stations in the area nearby these active leads (Cox et al., 2021). Also observed continuously from the tower were mass fluxes of drifting and blowing snow at an average height of 0.1 m using a snow particle counter (SPC-95, Niigata Electric Co., Ltd.; Wagner et al., 2022). Surface snow samples from various locations were collected approximately every other day as part of the snow chemistry program and stable water isotopes were subsequently measured.

We studied the snow loss in four of the leads (described in Section 2.2) that formed in a range of conditions. We collected 7–14 ice cores with a diameter of 9 cm from each lead along transects perpendicular and parallel to the leads with a spacing of 1–2.5 m between cores. One or two cores from each lead were vertically sectioned into 5 cm samples in the field and the remainder were whole core samples. We recorded ice thickness, snow depth, freeboard, core length, and visual stratigraphy (locations and thicknesses of granular ice layers) in the field. Onboard Polarstern, we melted each sample and homogenized it before measuring salinity (practical salinity scale) with a YSI Model 30 and completely filling and sealing a 20 mL subsample in a HDPE vial. The δ^{18}O of the subsamples were determined in the central laboratory of the Swiss Federal Institute for Forest, Snow and Landscape, Birmensdorf, Switzerland with an Isotopic Water Analyzer IWA-45-ER (ABB - Los Gatos Research Inc., US). Measurement uncertainty for δ^{18}O was ± 1‰, the precision ± 0.5‰. Samples were measured in duplicate and averaged. The quality control was conducted with three standards for δ^{18}O at 0.00‰, -12.34‰, and -55.50‰are presented as per mil difference relative to VSMOW (‰, Vienna Standard Mean Ocean Water).

2.2 Lead descriptions

Information on the four leads is presented in Table 1 and Sections 2.2.1–2.2.4. Supporting information includes additional details on sampling (Section S1) and maps of lead locations (Figure S1).

Table 1. Lead characteristics

Lead	Date opened	Air temperature range[a] (°C)	Wind speed range[a] ($m\ s^{-1}$)	Relative wind direction inter-quartile[a,b] (°)	Mean blowing snow flux[a] ($kg\ m^{-2}\ s{-1}$)	Date sampled	Width[c] (m)	Rafted[c]	Transect Type(s)	Core spacing (m)	# of cores	# of sectioned cores
SL[d]	25 March	[-28.8, -24.1]	[6.5, 10.8]	[21, 32]	0.000357	15 April	40	Yes	Perpendicular and parallel	1	12	1
SL[d]	29 March	[-29.7, -24.2]	[3.0, 8.3]	[348, 357]	0.000498	15 April	40	Yes	Perpendicular and parallel	1	12	1
T	4 April	[-26.7, -21.3]	[3.3, 10.0]	[43, 73]	0.000008	15 April	8	Yes	Perpendicular	1	8	2
M	23 March	[-29.8, -25.5]	[0.6, 2.9]	[101, 145]	0.000000	18 April	23	No	Perpendicular and parallel	1–2.5	14	1
A	19 April	[-15.3, 0.0]	[0.6, 15.7]	[11, 214]	0.068550	24 & 28 April	6	No	Perpendicular	1	7	2

[a]When the lead was open. [b]Relative wind direction follows the meteorological convention (direction wind is coming from, angles increasing clockwise) and has been rotated so a wind directly perpendicular to the lead is 0° or 180°, and directly parallel to the lead is 90° or 270°.
[c]When the lead was sampled. [d]There were two possible dates when the ice sampled in SL lead could have formed as described in Section 2.2.1

2.2.1 SL lead

The SL lead opened for the first time on 11 March and experienced numerous subsequent cycles of opening and refreezing followed by ridging and rafting. The ice we sampled formed in lead opening events on either 25–26 or 29–30 March. Although the date of ice formation is not known, the surface meteorology was similar during the two opening periods, with air temperatures close to climatological values (Rinke et al., 2021). We have combined these time periods in subsequent analysis (e.g. Figure 2a). Most ice cores contained a granular layer 3 cm thick at 15 cm depth (Figure 1a). This layer, combined with observations that the lead contracted after opening, indicated that the ice rafted after formation.

2.2.2 M lead

The M lead opened around 4:00 UTC on 23 March. Within a few hours of opening, the lead was covered by a thin layer of nilas. Between 29 March and 1 April, a closing event reduced the lead's width by approximately half to 8 meters wide. Afterwards the lead remained quiescent. Most cores contained a granular layer 1 cm thick at 32 cm depth (Figure 1b), indicating that the ice rafted after formation.

2.2.3 T lead

The T lead opened around 0:00 UTC 4 April. During 5–8 April, ice dynamics occurred in the center of the T lead but not where we would subsequently collect samples from. The T lead was split in the middle by a crack running parallel to the lead that opened the morning we sampled. Unfortunately, we were unable to access the ice on the upwind (at the time of lead formation) half of the lead on 15 April and this ice ridged in the following days.

2.2.4 A lead

The A lead opened around 8:20 UTC 19 April during a warm air advection event associated with extreme warmth (Rinke et al., 2021), precipitation, and high winds originating from a cyclone moving northward from the Greenland Sea. During 19–20 April, the open water we observed in leads was not rapidly freezing. We visually estimated that the open water fraction in the area within 1 km of Polarstern was approximately 0.03.

Within a 50 km radius of Polarstern, ice drift derived from subsequent SAR scenes indicates that divergent ice motion opened new leads covering approximately 0.02 of the area (these measurements do not preclude the persistence of open water from prior days).

Retrievals of precipitation from above the height of blowing snow based on a 35-GHz vertically-pointing radar mounted on the Polarstern deck (Matrosov et al., 2022) indicate 1.04 cm of liquid-equivalent snowfall from 16–22 April(Matrosov et al., 2022). Blowing snow picked up around 0530 UTC on 20 April. The three stations on level ice near Polarstern observed accumulation generally coinciding with pulses of precipitation (documented by radar reflectivities), followed shortly by ablation. At each station, winds eroded 100% of this new snow, but none of the preexisting snow, resulting in no net change in the surface height after the event. This suggests that much of the blowing snow during the A lead event was from concurrent precipitation.

Cores from the A lead on 24 April (Figure 1d) generally comprised about 27 cm of very soft ice overlying 31–37 cm of slush. Ice thickness measurements indicated that there were 10–20 cm of slush below this that the corer was unable to collect. The ice had a distinctive layer-cake-like structure with alternating light and dark 1–3 cm thick layers. We revisited the A lead on 28 April and collected a single core. This core was considerably more solid than those collected four days prior, but was otherwise similar.

2.3 Analysis of snow mass in leads

Following Jeffries et al. (1994); Granskog et al. (2017); Tian et al. (2020), the δ^{18}O in a sample of sea ice is a mixture, by mass, of the δ^{18}O of pure snow—which we denote $\delta_{s,l}$ for lead l—and the δ^{18}O of snow-free sea ice—which we denote δ_{ref} (same notation as Granskog et al., 2017). Additionally, we represent the measurement uncertainty of the δ^{18}O measurement (Section 2.1) as gaussian, uncorrelated noise—which we denote $\epsilon_{l,i}$ for sample i from lead l—with a standard deviation: $\sigma_\delta = 0.5$ ‰. Equations 1 and 2 represent this model:

$$\delta_{l,i} = \frac{s_{l,i}}{t_{l,i}}\delta_{s,l} + \left(1 - \frac{s_{l,i}}{t_{l,i}}\right)\delta_{ref} + \epsilon_{l,i} \tag{1}$$

$$\epsilon_{l,i} \sim N(0, \sigma_\delta^2) \tag{2}$$

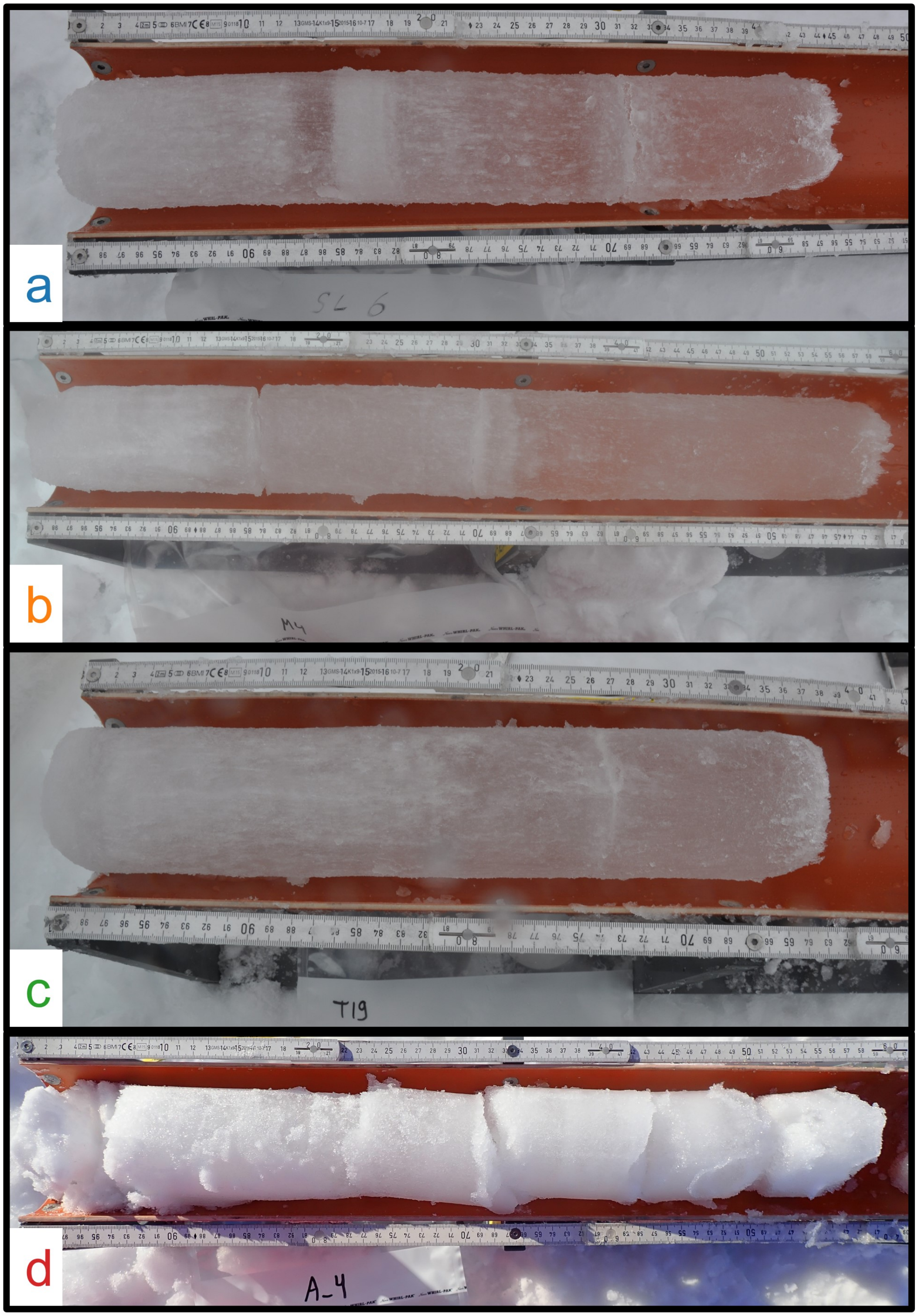

Figure 1. Representative ice cores from leads SL (a), M (b), T (c), and A (d). The top of each core is to the left. The SL and M cores contain granular layers around 15 and 30 cm respectively. The T core contains no granular layers below the top (the feature at 28 cm is a crack), and the A core is entirely opaque.

where $s_{l,i}$ is the SWE in the sample and $t_{l,i}$ is the total water equivalent of the sample. $\frac{s_{l,i}}{t_{l,i}}$ is the mass fraction of snow in the ice.

The δ^{18}O of snow-free ice (δ_{ref}) is higher than that of pure sea water because fractionation during the freezing process enriches it in ^{18}O (K. Moore et al., 2017; Tian et al., 2020). We follow Granskog et al. (2017) and use the bottom ice samples of the sectioned cores (defined as ice below the lowest granular ice) to determine δ_{ref}. To account for the measurement uncertainty, we represent δ_{ref} as a normal distribution whose mean (μ_{ref}) and standard deviation (τ_{ref}) are estimated from the bottom ice samples via Bayesian inference with a noninformative prior (Gelman et al., 2021, Chapter 2.5).

The δ^{18}O of snow ($\delta_{s,l}$) varies depending on the provenance of the snow. In particular, snow precipitated from warmer air masses (e.g. the 16–21 April warm air intrusions) is less depleted in ^{18}O (has less negative δ^{18}O) than snow from colder air masses. For the A lead event, we identified two surface snow samples that accumulated contemporaneously with snow blowing into A lead. We represent $\delta_{s,A}$ as a normal distribution whose mean ($\mu_{s,A}$) and standard deviation ($\tau_{s,A}$) are estimated from these surface snow samples in the same manner as δ_{ref}.

For the snow blown into the SL, M, and T leads, we could not unambiguously identify surface snow samples that accumulated during each event. The blowing snow during these events was likely re-mobilized snow. Eleven surface snow samples were collected from a week before the first lead opened to a week after the last lead refroze (16 March–12 April). To account for the fact that we do not know the precise provenance of the snow blown into these leads, we estimated the mean ($\mu_{s,(SL,M,T)}$) and standard deviation ($\tau_{s,(SL,M,T)}$) of $\delta_{s,(SL,M,T)}$ as the sample mean and standard deviation of these eleven samples. In this case, the uncertainty of the provenance greatly exceeds the measurement uncertainty.

We apply Bayes rule (Bayes & Price, 1763) to estimate the probability density of SWE in each core given its δ^{18}O measurement ($\mathbb{P}(s_{l,i} \mid \delta_{l,i})$; Equation 3). For sectioned cores, we computed the weighted-average (by section length) δ^{18}O for the core from the sections. The likelihood ($\mathbb{P}(\delta_{l,i} \mid s_{l,i})$; Equations 4–6) follows from the mixture model (Equations 1 & 2). We have no prior information about the snow mass in these leads except that it is non-negative and cannot exceed the total mass of the ice ($t_{l,i}$). Thus we represent our prior ($\mathbb{P}(s_{l,i})$; Equation 7) as a uniform distribution on this domain. We numerically estimate $\mathbb{P}(s_{l,i} \mid \delta_{l,i})$ through grid sampling (Gelman et al., 2021, Chapter 10.3). The probability density of the mean SWE in each lead given the N samples from that lead ($\mathbb{P}(s_l \mid \delta_{l,1}, \delta_{l,2}, ..., \delta_{l,N})$; Equation 8) is the conflation (Hill, 2011) of the sample probability densities ($\mathbb{P}(s_{l,i} \mid \delta_{l,i})$).

$$\mathbb{P}(s_{l,i} \mid \delta_{l,i}) \propto \mathbb{P}(\delta_{l,i} \mid s_{l,i})\mathbb{P}(s_{l,i}) \tag{3}$$

$$\mathbb{P}(\delta_{l,i} \mid s_{l,i}) = \frac{1}{\sigma_{l,i}\sqrt{2\pi}} \exp\left(\frac{-(\delta_{l,i} - \mu_{l,i})^2}{2\sigma_{l,i}^2}\right) \tag{4}$$

$$\mu_{l,i} = \frac{s_{l,i}}{t_{l,i}}\mu_{s,l} + \left(1 - \frac{s_{l,i}}{t_{l,i}}\right)\mu_{ref} \tag{5}$$

$$\sigma_{l,i}^2 = \left(\frac{s_{l,i}}{t_{l,i}}\right)^2 \tau_{s,l}^2 + \left(1 - \frac{s_{l,i}}{t_{l,i}}\right)^2 \tau_{ref}^2 + \sigma_\delta^2 \tag{6}$$

$$\mathbb{P}(s_{l,i}) = U(0, t_{l,i}) \tag{7}$$

$$\mathbb{P}(s_l \mid \delta_{l,1}, \delta_{l,2}, ..., \delta_{l,N}) \propto \prod_{i=1}^{N} \mathbb{P}(s_{l,i} \mid \delta_{l,i}) \tag{8}$$

3 Results

During the A lead event, peak air temperatures reached ∼0 °C (16 °C warmer than the November to April average) and it coincided with one of the largest blowing snow events (97th percentile) of December through April (Figure 2a,b). In contrast, the SL and T leads formed during typical temperature, wind, and blowing snow conditions (blowing snow at 66th and 33rd percentiles respectively; Figure 2a,b). During the formation of the M lead wind speeds were calmer than usual, temperatures were typical, and the blowing snow was at the 9th percentile.

The mean δ^{18}O of the A lead (−8.9 ‰) was considerably lower than that of the SL, M, and T leads (1.2, 2.0, and 2.4 ‰respectively). The δ^{18}O of snow-free ice (δ_{ref}) was 2.24 ± 0.30 ‰(all plus-minus at the 95% confidence level; solid black line in Figure 2c). For the A lead event $\delta_{s,A}$ was -14.3 ± 0.70 ‰(dotted red line in Figure 2c). For the other leads $\delta_{s,(SL,M,T)}$ was -23.0 ± 14.3 ‰(dotted black line in Figure 2c). See supporting information (Section S2 and Tables S1&S2) for more information on δ^{18}O of snow and snow-free ice.

The SWE in the A lead (35.0 ± 1.1 cm; Figure 2d) was approximately sixteen times greater per unit area than that in the SL lead (2.2 ± 0.7 cm)—the next highest. The M lead contained just 0.6 cm of SWE (95% credible interval 0.1–1.2 cm). Given the low winds and minimal blowing snow, much of this must have been interred by rafting. Finally, we found minimal—if any—SWE in the T lead (95% credible interval 0.0–0.4 cm). The mean snow percentages, by mass, in the A, SL, M, and T leads were 67.5%, 3.8%, 1.1%, and 0.3% respectively.

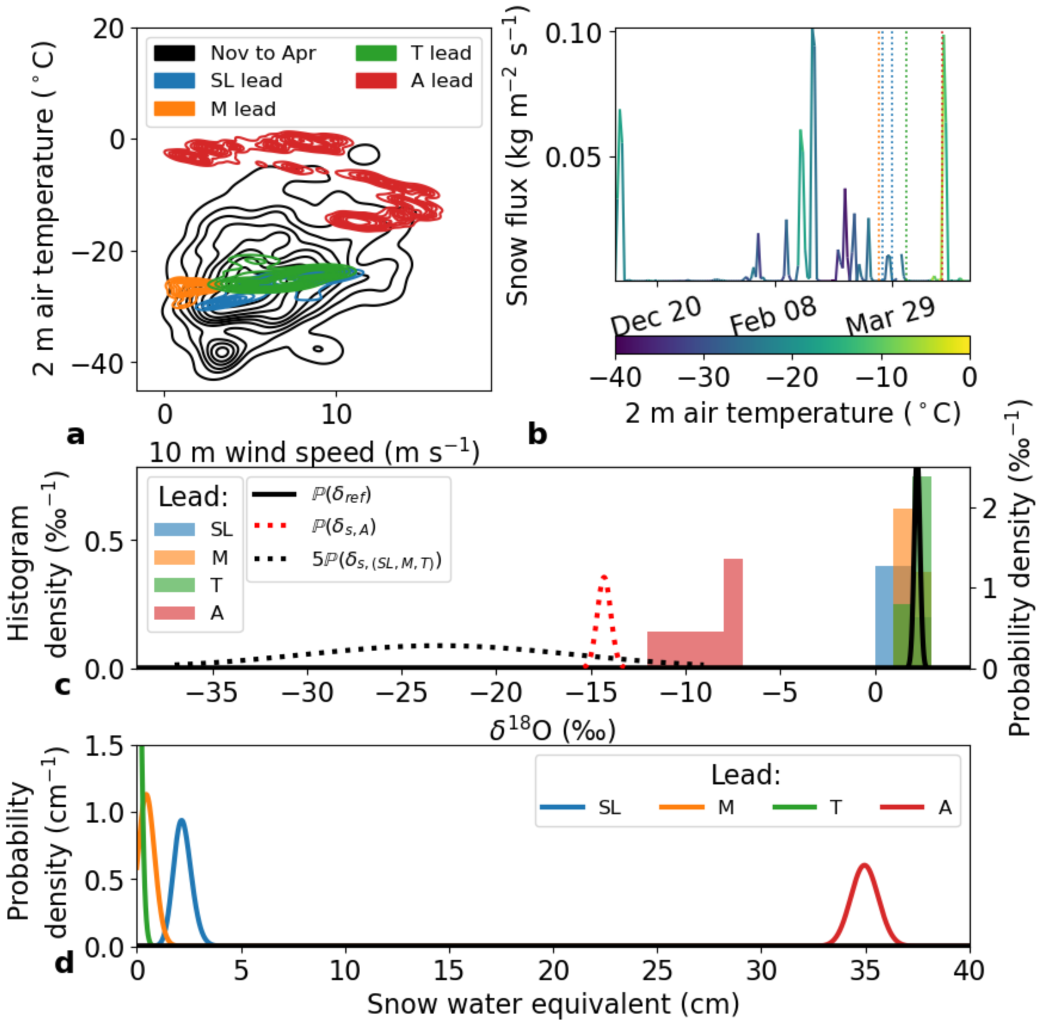

Figure 2. (a) the distribution of 10 m wind speed and 2 m air temperature for November to April at MOSAiC (black contours) with the distributions at the time of formation for each lead (colored contours). Contours indicate 10% density isolines. (b) daily mean snow mass flux measured nominally 10 cm above the surface, colored by air temperature. Formation dates of leads are indicated by vertical dotted lines (same colors as a,c,d). Both possible formation dates for ice in SL are indicated. (c) histograms δ^{18}O measurements for each lead (left axis) and distributions of δ^{18}O for snow and snow-free ice (right axis). (d) probability distributions of mean SWE in each lead.

The open water fraction during the A lead event was approximately 0.03 within 1 km of Polarstern and 0.02 with 50 km (Section 2.2.4). Thus, if the snow loss into A lead were typical of the event, snow loss may have reduced the snow budget by approximately 0.7–1.1 cm SWE. The other three lead events had a negligible impact on the snow budget.

4 Discussion

4.1 Minimal snow loss in typical wintertime conditions

Our results suggest that in typical wintertime conditions (characterized by the SL and T leads), minimal snow is lost into open water leads in the Arctic pack ice. First, at MOSAiC major blowing snow events—like the A lead event—were responsible for most of the blowing snow flux near the surface, but they occurred rarely and appear limited by the frequency of precipitation events. The ten days (6.6% of the data) with the highest blowing snow flux at MOSAiC accounted for 70% of the total cumulative blowing snow flux. All but one of these days came during or immediately after the five major snowfall events on MOSAiC (Wagner et al., 2022). Little snow is likely to be deposited in leads outside of a major blowing snow event. Second, at typical wintertime air temperatures, open water in leads rapidly refreezes—limiting snow loss. We discuss this process in more detail in Section 4.3. From November through April, only 4.3% of days had mean air temperatures above $-10°$C: two days in mid-November and six days in April (including the A lead event). Unfortunately, neither blowing snow flux data nor δ^{18}O lead ice samples are available for the mid-November event, so we cannot assess the amount of snow loss into leads. But it was potentially a high snow loss into leads event due to high wind speeds (mean 10.6 m s^{-1} on November 16) and observations of open water around the Polarstern. Besides the A lead and possibly mid-November events, the impact of snow loss into leads on the snow mass budget was likely minor. von Albedyll et al. (2022) estimated that from 14 October to 17 April, ice growth in leads contributed 0.1 m to the mean ice thickness. The mean snow percentages in our typical leads ranged from 0.3% (T lead) to 3.8% (SL lead). If these snow percentages were characteristic of ice grown in leads, then snow loss into typical wintertime leads consumed 0.02–0.34 cm SWE or approximately 0.2–3.2% of the total annual snow precipitation (Wagner et al., 2022).

4.2 Significant snow loss in exceptional conditions

If there is a recent snowfall, high winds, and open water remains unfrozen (due to high temperatures), a significant amount of snow can be lost into leads, even at open water fractions under 0.05. At MOSAiC, approximately 1.04 cm SWE precipitated immediately before and during the A lead event and 9.8–11.4 cm SWE precipitated at MOSAiC throughout the accumulation season (Matrosov et al., 2022; Wagner et al., 2022). Thus, snow loss into open water during the A lead event may have consumed 65–100% of the recent precipitation and 6–10% of the total annual snow precipitation. This is consistent with the observation that no net accumulation occurred at the three meteorological stations (Section 2.2.4).

The A lead event was associated with a cyclone and warm air intrusion that advected warm air from the Atlantic and produced record-breaking warm and moist atmospheric conditions at the MOSAiC site (Rinke et al., 2021). While the April 2020 event was extreme, warming events are possibly becoming more common (G. W. K. Moore, 2016). The frequency of winter warming events North of 85°N roughly doubled from 1980 to 2015 (Graham et al., 2017). Further research is needed to explore the connections between snow loss into leads, cyclones, and warm air intrusions—and how these events might change snow loss in a changing climate.

4.3 Impacts of temperature on the duration of open water in leads

Once the surface of a lead is frozen, snow cannot directly enter open water. Due to enhanced turbulent heat flux (Andreas & Cash, 1999), leads under colder air freeze faster (Figure 3a). For example, on 11 March at an air temperature of −25 °C, we observed a thin ice skin form on a 1–2 m wide lead within 20 minutes. This lead was sufficiently refrozen to support snow on top of it within 2 hours (Figure 3b–d). In contrast, the leads during the A lead event stayed unfrozen for two days, likely due to the near-freezing air temperature suppressing the turbulent heat flux. Accounting for only turbulent heat fluxes (Andreas & Cash, 1999), a hypothetical 20-m-wide lead under a wind speed of 6 m s^{-1} could freeze 3.6 times faster at an air temperature of −24.6 °C (the November to April mean) than at a temperature of −7.8 °C (the A lead event mean; Figure 3a). Given a constant snow flux, the cold lead would consume 72% less snow than the warm one. The exact values change slightly with our assumptions about lead width and wind speed, but the overall pattern is that the duration of open water in leads increases dramatically for air temperatures above approximately $-10°C$.

Accounting for the impacts of air temperature on the duration of open water in leads may be important for models and data assimilation products representing snow loss into leads. For example, some sea ice concentration products (e.g., Comiso, 1986) misclassify thin ice as open water (Ivanova et al., 2015). Utilizing such products without accounting for the duration of open water could overestimate snow loss into leads.

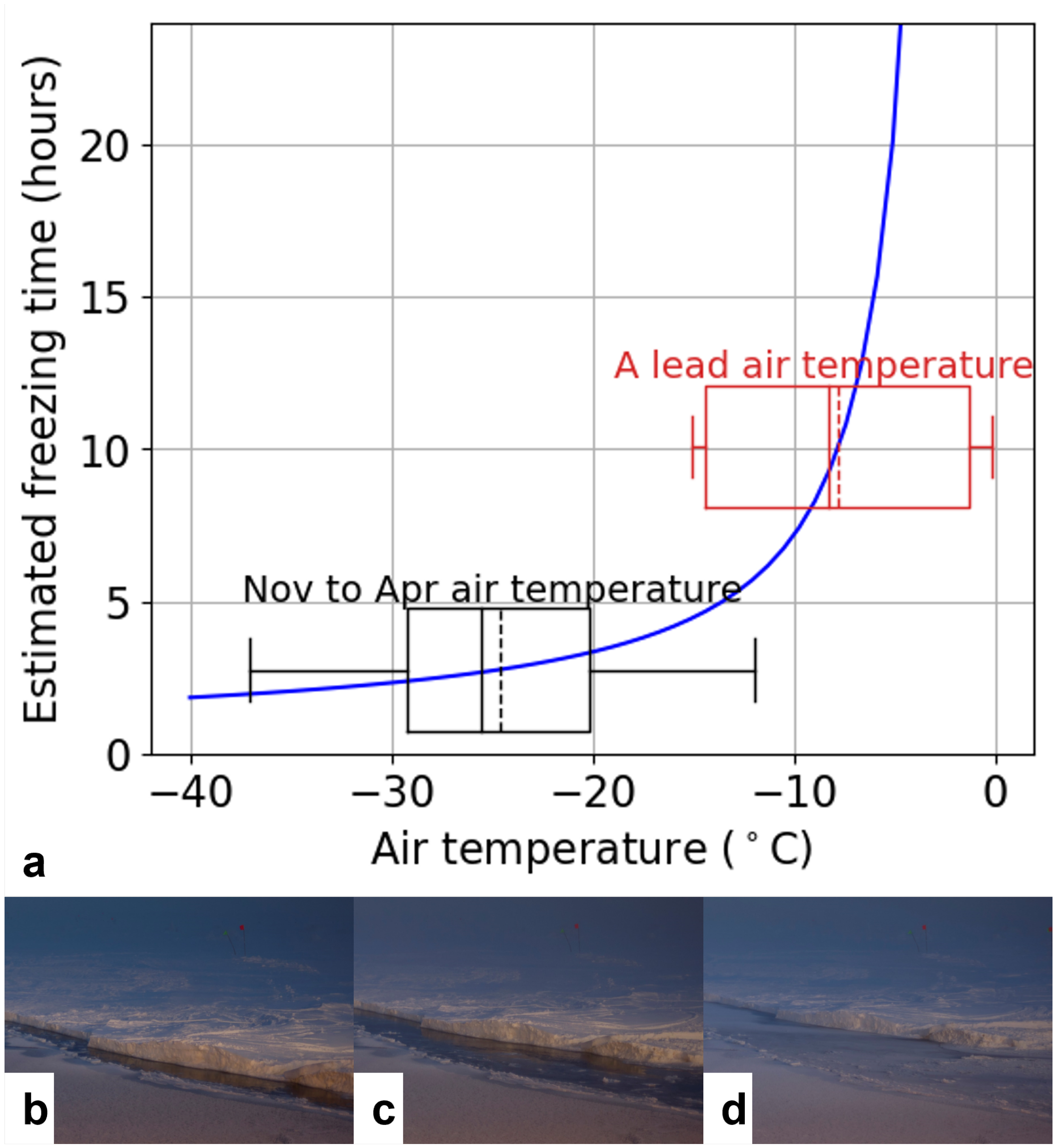

Figure 3. (a) estimated time required to freeze 3 cm of ice thickness in a 20-m-wide lead at a wind speed of 6 m s^{-1} for a given air temperature, only accounting for turbulent heat flux (estimated from Andreas & Cash, 1999). Boxes show interquartile ranges and whiskers show 90% ranges of air temperatures at MOSAiC. (b–d) Images of a freezing lead on MOSAiC. In (b) the ice has just opened up, exposing open water between the mature ice and the young ice (closer to the camera) which had formed a few hours prior. Within 20 minutes, (c) shows that a thin skim of ice has frozen over the open water (the mature ice has also retreated exposing more open water). Within 2 hours, (d) shows that this new ice is sufficiently solid to accumulate snow on top of it.

4.4 Outlook

Further work is needed to quantify the relationship between air temperature and snow loss into open water. In particular, observations of snow loss into leads during major blowing snow events at a range of air temperatures are needed. One limitation of this work is that we do not have ice samples from leads that formed during cold major blowing snow events. This temperature dependence could also be considered in models that represent snow loss into leads (e.g. Hunke et al., 2017; Petty et al., 2018), and it is important that models accurately simulate freezing times. Additionally, the net impacts of snow loss into leads on the ice mass budget are uncertain. The immediate impact of snow in leads on the ice budget is positive (the snow turns into ice), but the net effect may depend on the timing of snow loss events. If there were less snow on Arctic sea ice, it would increase thermodynamic ice growth in the winter (Maykut & Untersteiner, 1971; Sturm et al., 2002) but reduce the albedo (Perovich & Elder, 2002; Perovich & Polashenski, 2012), which increases ice melt in the summer. Thus, autumn snow loss events may increase the ice mass budget whereas spring snow loss events likely decrease it. Further observations and modeling are needed to investigate these competing effects.

5 Conclusions

We presented the first direct observations of snow loss into leads in the Arctic from four leads at MOSAiC. Three leads formed under typical, cold winter conditions and contained <2.9 cm SWE. Under typical winter conditions the impact of leads on the snow budget is likely minor. However, one lead contained 35.0 ± 1.1 cm SWE and was associated with a cyclone which delivered snowfall, high winds, and record-breaking warm temperatures. During this event, open water may have consumed 65–100% of recent snow precipitation and approximately 6–10% of annual snow precipitation. The frequency of such extreme events may be important for the snow budget on Arctic sea ice. Finally, this event highlighted that the duration of open water in leads, which increases dramatically with warmer air temperature, may be an underappreciated factor in how much snow can be lost into leads.

6 Open Research

Data from lead cores is available at Clemens-Sewall et al. (2022). Surface meteorology data are available at Cox et al. (2021). Snow surface isotope data are available at Macfarlane et al. (2022). The blowing snow flux data are currently in the process of data archiving at the UK Polar Data Centre. They will be published before publication of this manuscript and will be cited herein.

Acknowledgments

Data used in this manuscript were produced as part of the international MOSAiC project with the tag MOSAiC20192020 and the Project_ID: AWI_PS122_00. We thank all people involved in the expedition of the research vessel Polarstern (Knust, 2017) during MOSAiC in 2019–2020 as listed in Nixdorf et al. (2021). In particular, we thank Eric Brossier, Thomas Olufson, Delphin Ruché, and Saga Svavarsdottir, for their capable assistance in the field. Thank you to Manuel Ernst for assistance with the time lapse imagery.

DCS, CP, and DP were supported by NSF OPP-1724540. MMF was supported by UK Natural Environment Research Council grant NE/S00257X/1. MAG was supported by the Norwegian Polar Institute and funding from the Research Council of Norway for project HAVOC (grant no 280292). JS received funding from the Swiss National Science Foundation (grant no. 188478) and the Swiss Polar Institute. JS holds the Ingvar Kamprad Chair for Extreme Environments Research sponsored by Ferring Pharmaceuticals. JKH was supported by NSF OPP-1722729. LvA was funded by the Alfred-Wegener-Institut, Helmholtz-Zentrum für Polar- und Meeresforschung through the project AWI_ICE. SWF was supported by the National Aeronautics and Space Administration Cryospheric Sciences Internal Scientist Funding Model (ISFM). ARM was supported by the WSL Institute for Snow and Avalanche Research SLF. WSL_201812N1678. Funder ID: `http://dx.doi.org/10.13039/501100015742`, the Swiss Polar Institute (SPI reference DIRCR-2018-003) Funder ID `http://dx.doi.org/10.13039/501100015594` and the European Union's Horizon 2020 research and innovation program projects ARICE (grant 730965) for berth fees associated with the participation of the DEARice project. SA was supported by the German Research Council (DFG) in the framework of the priority program "Antarctic Research with comparative investigations in the Arctic ice areas" (grant nos. SPP1158 and AR1236/1) and by the Alfred-Wegener-Institut, Helmholtz-Zentrum für Polar- und Meeresforschung. CJC and meteorological data were supported by the National Science Foundation (grant no. OPP-1724551) and by NOAA's Physical Sciences Laboratory (PSL) and Global Ocean Monitoring and Observing Program (GOMO).

References

Andreas, E. L., & Cash, B. A. (1999). Convective heat transfer over wintertime leads and polynyas. *Journal of Geophysical Research: Oceans*, *104*(C11), 25721–25734. Retrieved 2022-07-15, from https://onlinelibrary.wiley.com/doi/abs/10.1029/1999JC900241 (_eprint: https://onlinelibrary.wiley.com/doi/pdf/10.1029/1999JC900241) doi: 10.1029/1999JC900241

Arndt, S., Haas, C., Meyer, H., Peeken, I., & Krumpen, T. (2021, August). Recent observations of superimposed ice and snow ice on sea ice in the northwestern Weddell Sea. *The Cryosphere*, *15*(9), 4165–4178. Retrieved 2022-06-19, from https://tc.copernicus.org/articles/15/4165/2021/ (Publisher: Copernicus GmbH) doi: 10.5194/tc-15-4165-2021

Bayes, T., & Price, n. (1763, January). LII. An essay towards solving a problem in the doctrine of chances. By the late Rev. Mr. Bayes, F. R. S. communicated by Mr. Price, in a letter to John Canton, A. M. F. R. S. *Philosophical Transactions of the Royal Society of London*, *53*, 370–418. Retrieved 2022-08-16, from https://royalsocietypublishing.org/doi/10.1098/rstl.1763.0053 (Publisher: Royal Society) doi: 10.1098/rstl.1763.0053

Clemens-Sewall, D., Macfarlane, A., Fons, S., Granskog, M., Hutchings, J., & Schmale, J. (2022). Salinity and Stable Water Isotopes for Ice Cores in Leads during Leg 3 of the Multidisciplinary drifting Observatory for the Study of Arctic Climate 2020. *Arctic Data Center*. Retrieved 2023-01-08, from https://arcticdata.io/catalog/view/doi%3A10.18739%2FA23N20G15 (Publisher: Arctic Data Center) doi: 10.18739/A23N20G15

Comiso, J. C. (1986). Characteristics of Arctic winter sea ice from satellite multispectral microwave observations. *Journal of Geophysical Research: Oceans*, *91*(C1), 975–994. Retrieved 2022-08-17, from https://onlinelibrary.wiley.com/doi/abs/10.1029/JC091iC01p00975 (_eprint: https://onlinelibrary.wiley.com/doi/pdf/10.1029/JC091iC01p00975) doi: 10.1029/JC091iC01p00975

Cox, C., Gallagher, M., Shupe, M., Persson, O., Solomon, A., Blomquist, B., ... Uttal, T. (2021). 10-meter (m) meteorological flux tower measurements (Level 1 Raw), Multidisciplinary Drifting Observatory for the Study of Arctic Climate (MOSAiC), central Arctic, October 2019 - September 2020. *Arctic Data Center*. Retrieved 2022-08-17, from https://arcticdata.io/catalog/view/doi%3A10.18739%2FA2VM42Z5F (type: dataset) doi: 10.18739/A2VM42Z5F

Dansgaard, W. (1953). The Abundance of O18 in Atmospheric Water and Water Vapour. *Tellus*, *5*(4), 461–469. Retrieved 2022-06-19, from https://onlinelibrary.wiley.com/doi/abs/10.1111/j.2153-3490.1953.tb01076.x (_eprint: https://onlinelibrary.wiley.com/doi/pdf/10.1111/j.2153-3490.1953.tb01076.x) doi: 10.1111/j.2153-3490.1953.tb01076.x

Gelman, A., Carlin, J. B., Stern, H. S., Dunson, D. B., Vehtari, A., & Rubin, D. B. (2021). *Bayesian Data Analysis Third edition (with errors fixed as of 15 February 2021)* (3rd ed.). Columbia University Department of Statistics. Retrieved from http://www.stat.columbia.edu/~gelman/book/

Graham, R. M., Cohen, L., Petty, A. A., Boisvert, L. N., Rinke, A., Hudson, S. R., … Granskog, M. A. (2017). Increasing frequency and duration of Arctic winter warming events. *Geophysical Research Letters*, *44*(13), 6974–6983. Retrieved 2022-07-23, from https://onlinelibrary.wiley.com/doi/abs/10.1002/2017GL073395 (_eprint: https://onlinelibrary.wiley.com/doi/pdf/10.1002/2017GL073395) doi: 10.1002/2017GL073395

Granskog, M. A., Leppäranta, M., Kawamura, T., Ehn, J., & Shirasawa, K. (2004). Seasonal development of the properties and composition of landfast sea ice in the Gulf of Finland, the Baltic Sea. *Journal of Geophysical Research: Oceans*, *109*(C2). Retrieved 2022-06-19, from https://onlinelibrary.wiley.com/doi/abs/10.1029/2003JC001874 (_eprint: https://onlinelibrary.wiley.com/doi/pdf/10.1029/2003JC001874) doi: 10.1029/2003JC001874

Granskog, M. A., Martma, T. A., & Vaikmäe, R. A. (2003). Development, structure and composition of land-fast sea ice in the northern Baltic Sea. *Journal of Glaciology*, *49*(164), 139–148. Retrieved 2022-06-19, from https://www.cambridge.org/core/journals/journal-of-glaciology/article/development-structure-and-composition-of-landfast-sea-ice-in-the-northern-baltic-sea/2CBF18DB118AC3BDA1993FBCD207C2C7 (Publisher: Cambridge University Press) doi: 10.3189/172756503781830872

Granskog, M. A., Rösel, A., Dodd, P. A., Divine, D., Gerland, S., Martma, T., & Leng, M. J. (2017, March). Snow contribution to first-year and second-year Arctic sea ice mass balance north of Svalbard. *Journal of Geophysical Research: Oceans*, 2539–2549. Retrieved 2018-09-26, from https://agupubs.onlinelibrary.wiley.com/doi/abs/10.1002/2016JC012398%4010.1002/%28ISSN%292169-9291.NICE1 doi: 10.1002/2016JC012398@10.1002/(ISSN)2169-9291.NICE1

Hill, T. (2011, June). Conflations of probability distributions. *Transactions of the American Mathematical Society*, *363*(6), 3351–3372. Retrieved 2022-07-20, from https://www.ams.org/tran/2011-363-06/S0002-9947-2011-05340-7/ doi: 10.1090/S0002-9947-2011-05340-7

Hunke, E., Lipscomb, W., Jones, P., Turner, A., Jeffery, N., & Elliott, S. (2017, May). *CICE, The Los Alamos Sea Ice Model* (Tech. Rep. No. CICE; 005315WKSTN00). Los Alamos National Lab. (LANL), Los Alamos, NM (United States). Retrieved 2018-10-04, from https://www.osti.gov/biblio/1364126

Iacozza, J., & Ferguson, S. H. (2014, June). Spatio-temporal variability of snow over sea ice in western Hudson Bay, with reference to ringed seal pup survival. *Polar Biology*, *37*(6), 817–832. Retrieved 2022-06-19, from https://doi.org/10.1007/s00300-014-1484-z doi: 10.1007/s00300-014-1484-z

Ivanova, N., Pedersen, L. T., Tonboe, R. T., Kern, S., Heygster, G., Lavergne, T., … Shokr, M. (2015, September). Inter-comparison and evaluation of sea ice algorithms: towards further identification of challenges and optimal approach using passive microwave observations. *The Cryosphere*, *9*(5), 1797–1817. Retrieved 2022-08-16, from https://tc.copernicus.org/articles/9/1797/2015/ doi: 10.5194/tc-9-1797-2015

Jeffries, M. O., Krouse, H. R., Hurst-Cushing, B., & Maksym, T. (2001). Snow-ice accretion and snow-cover depletion on Antarctic first-year sea-ice floes. *Annals of Glaciology*, *33*, 51–60. Retrieved 2022-06-19, from https://www.cambridge.org/core/journals/annals-of-glaciology/article/snowice-accretion-and-snowcover-depletion-on-antarctic-firstyear-seaice-floes/B17C1E8ACA3EABF64F09DC3B2A80DB0D (Publisher: Cambridge University Press) doi: 10.3189/172756401781818266

Jeffries, M. O., Morris, K., Weeks, W. F., & Worby, A. P. (1997). Seasonal variations in the properties and structural composition of sea ice and snow cover in the Bellingshausen and Amundsen Seas, Antarctica. *Journal of Glaciology*, *43*(143), 138–151. Retrieved 2022-06-19, from `https://www.cambridge.org/core/journals/journal-of-glaciology/article/seasonal-variations-in-the-properties-and-structural-composition-of-sea-ice-and-snow-cover-in-the-bellingshausen-and-amundsen-seas-antarctica/D4475C2D538E87C677BB94FCDA38AF06` (Publisher: Cambridge University Press) doi: 10.3189/S0022143000002902

Jeffries, M. O., Shaw, R. A., Morris, K., Veazey, A. L., & Krouse, H. R. (1994, January). Crystal structure, stable isotopes (δ18O), and development of sea ice in the Ross, Amundsen, and Bellingshausen seas, Antarctica. *Journal of Geophysical Research: Oceans*, *99*(C1), 985–995. Retrieved 2018-10-17, from `https://agupubs.onlinelibrary.wiley.com/doi/abs/10.1029/93JC02057` doi: 10.1029/93JC02057

Kawamura, T., Shirasawa, K., Ishikawa, N., Lindfors, A., Rasmus, K., Granskog, M. A., . . . Vaikmäe, R. (2001). Time-series observations of the structure and properties of brackish ice in the Gulf of Finland. *Annals of Glaciology*, *33*, 1–4. Retrieved 2022-06-19, from `https://www.cambridge.org/core/journals/annals-of-glaciology/article/timeseries-observations-of-the-structure-and-properties-of-brackish-ice-in-the-gulf-of-finland/1DA61BE13E5F6A9184CACC1F513CF27C` (Publisher: Cambridge University Press) doi: 10.3189/172756401781818950

Knust, R. (2017, October). Polar Research and Supply Vessel POLARSTERN Operated by the Alfred-Wegener-Institute. *Journal of large-scale research facilities JLSRF*, *3*(0), A119. Retrieved 2021-10-28, from `http://jlsrf.org/index.php/lsf/article/view/163` (Number: 0) doi: 10.17815/jlsrf-3-163

Lecomte, O., Fichefet, T., Flocco, D., Schroeder, D., & Vancoppenolle, M. (2015, March). Interactions between wind-blown snow redistribution and melt ponds in a coupled ocean-sea ice model. *Ocean Modelling*, *87*, 67–80. Retrieved 2021-10-12, from `https://www.sciencedirect.com/science/article/pii/S1463500314001784` doi: 10.1016/j.ocemod.2014.12.003

Leonard, K. C., & Maksym, T. (2011). The importance of wind-blown snow redistribution to snow accumulation on Bellingshausen Sea ice. *Annals of Glaciology*, *52*(57), 271–278. Retrieved 2018-10-17, from https://www.cambridge.org/core/journals/annals-of-glaciology/article/importance-of-windblown-snow-redistribution-to-snow-accumulation-on-bellingshausen-sea-ice/4BDFC34361C599B250C071188A52FF0C doi: 10.3189/172756411795931651

Macfarlane, A. R., Schneebeli, M., Dadic, R., Wagner, D. N., Arndt, S., Clemens-Sewall, D., ... Brunello, C. F. (2022). Snowpit stable isotope profiles during the MOSAiC expedition. PANGAEA. Retrieved from https://doi.pangaea.de/10.1594/PANGAEA.952556 (Type: data set)

Matrosov, S. Y., Shupe, M. D., & Uttal, T. (2022, April). High temporal resolution estimates of Arctic snowfall rates emphasizing gauge and radar-based retrievals from the MOSAiC expedition. *Elementa: Science of the Anthropocene*, *10*(1), 00101. Retrieved 2022-08-17, from https://doi.org/10.1525/elementa.2021.00101 doi: 10.1525/elementa.2021.00101

Maykut, G. A., & Untersteiner, N. (1971). Some results from a time-dependent thermodynamic model of sea ice. *Journal of Geophysical Research*, *76*(6), 1550–1575. Retrieved 2019-01-03, from https://agupubs.onlinelibrary.wiley.com/doi/abs/10.1029/JC076i006p01550 doi: 10.1029/JC076i006p01550

Moore, G. W. K. (2016, December). The December 2015 North Pole Warming Event and the Increasing Occurrence of Such Events. *Scientific Reports*, *6*(1), 39084. Retrieved 2022-09-02, from https://www.nature.com/articles/srep39084 (Number: 1 Publisher: Nature Publishing Group) doi: 10.1038/srep39084

Moore, K., Fayek, M., Lemes, M., Rysgaard, S., & Holländer, H. M. (2017, October). Fractionation of hydrogen and oxygen in artificial sea ice with corrections for salinity for determining meteorological water content in bulk ice samples. *Cold Regions Science and Technology*, *142*, 93–99. Retrieved 2022-06-27, from https://www.sciencedirect.com/science/article/pii/S0165232X16302749 doi: 10.1016/j.coldregions.2017.07.011

Nicolaus, M., Arndt, S., Birnbaum, G., & Katlein, C. (2021, November). Visual panoramic photographs of the surface conditions during the MOSAiC campaign 2019/20. *PANGAEA*. Retrieved 2022-06-19, from https://doi.pangaea.de/10.1594/PANGAEA.938534 (Publisher: PANGAEA Type:

dataset) doi: 10.1594/PANGAEA.938534

Nicolaus, M., Perovich, D. K., Spreen, G., Granskog, M. A., von Albedyll, L., Angelopoulos, M., ... Wendisch, M. (2022, February). Overview of the MOSAiC expedition: Snow and sea ice. *Elementa: Science of the Anthropocene*, *10*(1), 000046. Retrieved 2022-02-07, from https://doi.org/10.1525/elementa.2021.000046 doi: 10.1525/elementa.2021.000046

Nixdorf, U., Dethloff, K., Rex, M., Shupe, M., Sommerfeld, A., Perovich, D. K., ... Boetius, A. (2021, September). MOSAiC Extended Acknowledgement. *Zenodo*. Retrieved 2021-10-22, from https://zenodo.org/record/5541624 (Publisher: Zenodo) doi: 10.5281/zenodo.5541624

Perovich, D. K., & Elder, B. (2002). Estimates of ocean heat flux at SHEBA. *Geophysical Research Letters*, *29*(9), 58–1–58–4. Retrieved 2020-01-27, from https://agupubs.onlinelibrary.wiley.com/doi/abs/10.1029/2001GL014171 doi: 10.1029/2001GL014171

Perovich, D. K., Grenfell, T. C., Light, B., & Hobbs, P. V. (2002). Seasonal evolution of the albedo of multiyear Arctic sea ice. *Journal of Geophysical Research: Oceans*, *107*(C10), SHE 20–1–SHE 20–13. Retrieved 2021-06-28, from https://agupubs.onlinelibrary.wiley.com/doi/abs/10.1029/2000JC000438 (_eprint: https://agupubs.onlinelibrary.wiley.com/doi/pdf/10.1029/2000JC000438) doi: 10.1029/2000JC000438

Perovich, D. K., & Polashenski, C. (2012). Albedo evolution of seasonal Arctic sea ice. *Geophysical Research Letters*, *39*(8). Retrieved 2022-06-19, from https://onlinelibrary.wiley.com/doi/abs/10.1029/2012GL051432 (_eprint: https://onlinelibrary.wiley.com/doi/pdf/10.1029/2012GL051432) doi: 10.1029/2012GL051432

Petty, A. A., Webster, M., Boisvert, L., & Markus, T. (2018, November). The NASA Eulerian Snow on Sea Ice Model (NESOSIM) v1.0: initial model development and analysis. *Geoscientific Model Development*, *11*(11), 4577–4602. Retrieved 2021-12-10, from https://gmd.copernicus.org/articles/11/4577/2018/ (Publisher: Copernicus GmbH) doi: 10.5194/gmd-11-4577-2018

Polashenski, C., Perovich, D., & Courville, Z. (2012, January). The mechanisms of sea ice melt pond formation and evolution. *Journal of Geophys-*

ical Research: Oceans, *117*(C1). Retrieved 2018-09-17, from https://agupubs.onlinelibrary.wiley.com/doi/abs/10.1029/2011JC007231 doi: 10.1029/2011JC007231

Rabe, B., Heuzé, C., Regnery, J., Aksenov, Y., Allerholt, J., Athanase, M., ... Zhu, J. (2022, February). Overview of the MOSAiC expedition: Physical oceanography. *Elementa: Science of the Anthropocene*, *10*(1), 00062. Retrieved 2022-06-19, from https://doi.org/10.1525/elementa.2021.00062 doi: 10.1525/elementa.2021.00062

Rinke, A., Cassano, J. J., Cassano, E. N., Jaiser, R., & Handorf, D. (2021, July). Meteorological conditions during the MOSAiC expedition: Normal or anomalous? *Elementa: Science of the Anthropocene*, *9*(1), 00023. Retrieved 2022-08-16, from https://doi.org/10.1525/elementa.2021.00023 doi: 10.1525/elementa.2021.00023

Shupe, M. D., Rex, M., Blomquist, B., Persson, P. O. G., Schmale, J., Uttal, T., ... Yue, F. (2022, February). Overview of the MOSAiC expedition: Atmosphere. *Elementa: Science of the Anthropocene*, *10*(1), 00060. Retrieved 2022-06-19, from https://doi.org/10.1525/elementa.2021.00060 doi: 10.1525/elementa.2021.00060

Sturm, M., Perovich, D. K., & Holmgren, J. (2002, October). Thermal conductivity and heat transfer through the snow on the ice of the Beaufort Sea. *Journal of Geophysical Research: Oceans*, *107*(C10), SHE 19–1–SHE 19–17. Retrieved 2018-09-06, from https://agupubs.onlinelibrary.wiley.com/doi/abs/10.1029/2000JC000409 doi: 10.1029/2000JC000409

Tian, L., Gao, Y., Weissling, B., & Ackley, S. F. (2020, December). Snow-ice contribution to the structure of sea ice in the Amundsen Sea, Antarctica. *Annals of Glaciology*, *61*(83), 369–378. Retrieved 2022-06-19, from https://www.cambridge.org/core/journals/annals-of-glaciology/article/snowice-contribution-to-the-structure-of-sea-ice-in-the-amundsen-sea-antarctica/DD59C59BE13F453C6309BEDFB4B57C43 (Publisher: Cambridge University Press) doi: 10.1017/aog.2020.55

von Albedyll, L., Hendricks, S., Grodofzig, R., Krumpen, T., Arndt, S., Belter, H. J., ... Haas, C. (2022, April). Thermodynamic and dynamic contributions to seasonal Arctic sea ice thickness distributions from airborne observations. *Elementa: Science of the Anthropocene*, *10*(1), 00074. Retrieved 2022-08-16, from https://doi.org/10.1525/elementa.2021.00074 doi: 10.1525/elementa.2021.00074

Wagner, D. N., Shupe, M. D., Cox, C., Persson, O. G., Uttal, T., Frey, M. M., ... Lehning, M. (2022, June). Snowfall and snow accumulation during the MOSAiC winter and spring seasons. *The Cryosphere*, *16*(6), 2373–2402. Retrieved 2022-06-30, from https://tc.copernicus.org/articles/16/2373/2022/ (Publisher: Copernicus GmbH) doi: 10.5194/tc-16-2373-2022

Warren, S. G. (2019, June). Optical properties of ice and snow. *Philosophical Transactions of the Royal Society A: Mathematical, Physical and Engineering Sciences*, *377*(2146), 20180161. Retrieved 2021-12-10, from https://royalsocietypublishing.org/doi/full/10.1098/rsta.2018.0161 (Publisher: Royal Society) doi: 10.1098/rsta.2018.0161

Figure 1.


a
SL 6
b
M4
c
T19
d
A_4

Figure 2.

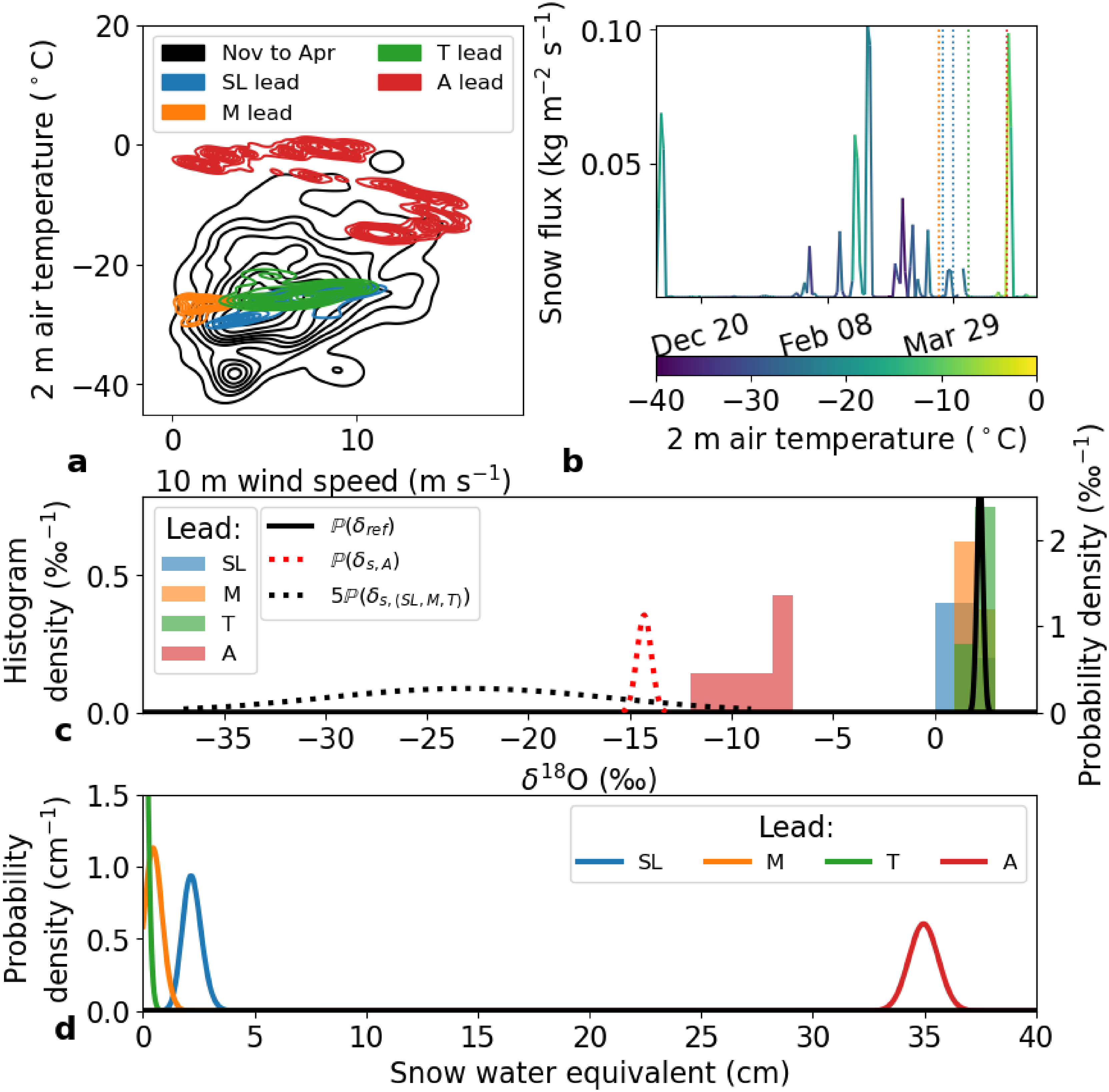

Nov to Apr
SL lead
M lead
T lead
A lead
2 m air temperature (°C)
10 m wind speed (m s^{-1})
a
Snow flux (kg m^{-2} s^{-1})
Dec 20
Feb 08
Mar 29
2 m air temperature (°C)
b
Lead:
SL
M
T
A
$\mathbb{P}(\delta_{ref})$
$\mathbb{P}(\delta_{s,A})$
$5\mathbb{P}(\delta_{s,(SL,M,T)})$
Histogram density (‰$^{-1}$)
Probability density (‰$^{-1}$)
δ^{18}O (‰)
c
Lead:
SL
M
T
A
Probability density (cm^{-1})
Snow water equivalent (cm)
d

Figure 3.

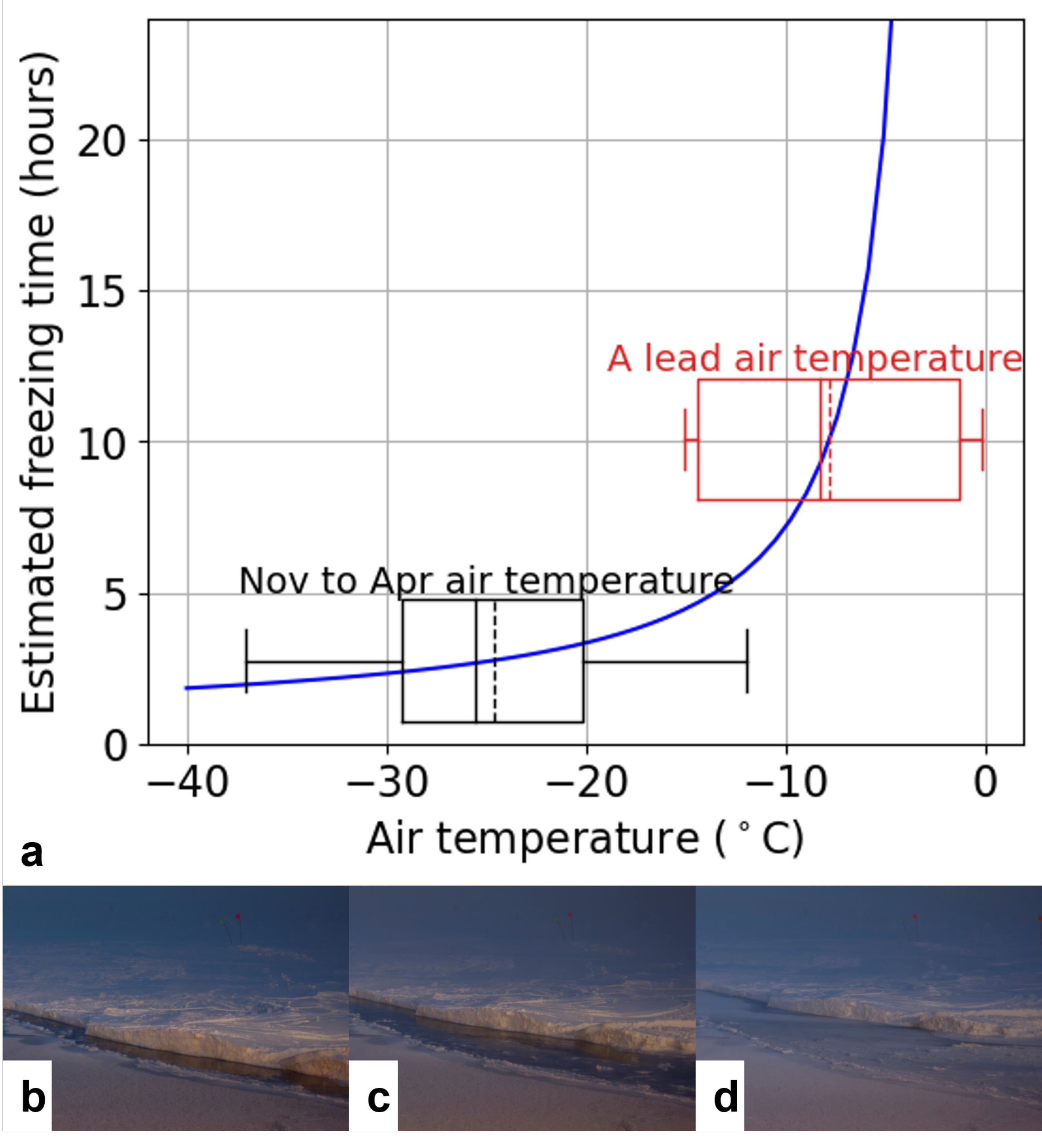

Estimated freezing time (hours)
20
15
10
5
0
−40
−30
−20
−10
0
Air temperature (°C)
A lead air temperature
Nov to Apr air temperature
a
b
c
d

Supporting Information for "Snow Loss into Leads in Arctic Sea Ice: Minimal in Typical Wintertime Conditions, but High During a Warm and Windy Snowfall Event"

David Clemens-Sewall[1], Chris Polashenski[1,2], Markus M. Frey[3], Christopher J. Cox[4], Mats A. Granskog[5], Amy R. Macfarlane[6], Steven W. Fons[7,8], Julia Schmale[9], Jennifer K. Hutchings[10], Luisa von Albedyll[11], Stefanie Arndt[11], Martin Schneebeli[6], Don Perovich[1]

[1]Thayer School of Engineering, Dartmouth College, Hanover, NH, USA

[2]Cold Regions Research and Engineering Laboratory, US Army Corps of Engineers, Hanover, NH, USA

[3]British Antarctic Survey – Natural Environment Research Council, Cambridge, UK

[4]NOAA Physical Sciences Laboratory, Boulder, CO, USA

[5]Norwegian Polar Institute, Fram Centre, Tromsø, Norway

[6]WSL Institute for Snow and Avalanche Research SLF, Davos, Switzerland

[7]Cryospheric Sciences Laboratory, NASA Goddard Space Flight Center, Greenbelt, MD, USA

[8]Earth System Science Interdisciplinary Center, University of Maryland, College Park, MD, USA

[9]Extreme Environments Research Laboratory, École Polytechnique Fédérale de Lausanne, Sion, Switzerland

[10]College of Earth, Ocean, and Atmospheric Sciences, Oregon State University, Corvallis, OR, USA

[11]Alfred-Wegener-Institut, Helmholtz-Zentrum für Polar- und Meeresforschung, Bremerhaven, Germany

Contents of this file

1. Text S1 and S2
2. Figures S1 and S2
3. Tables S1 and S2

Introduction

The supporting information presented here includes ancillary details about the leads sampled (Section S1 and Figure S1) and the isotopic composition of snow-free ice and snow (Section S2, Figure S2, and Tables S1&S2). This information is also available with the published data set (Clemens-Sewall et al., 2022).

S1. Lead Descriptions

S1.1 SL Lead

The SL lead (named for 'Stern Lead') extended more than 1 km aft and starboard of Polarstern (Figure S1). On 15 April at approximately 84.32°N, 13.77°E, we collected 12 ice cores from two transects (sample spacing 2.5 m) in the SL lead approximately 100 m from the stern of Polarstern. At this location, the lead was approximately 40 m wide. In the upwind half(relative to the winds 25 and 29 March), there were two 10-m-wide, flat pans of ice. The pans were separated by separated by a 50 cm tall ridge. The downwind half was a mixture of ridges and rubble. All samples came from the two flat pans on the upwind half. One transect was perpendicular to the lead and extended 20 m from the upwind edge across both pans (we did not core the small ridge). The other transect ran for 12 m parallel to the lead and was approximately 5 m from the upwind edge of the lead.

The transects intersected in the middle of the upwind pan, and the ice core at this site (DC_SL_5) was vertically sectioned. All other cores were collected as bulk samples. Some cores were underlain by a gap layer of water and then additional rafted blocks of ice. In general we collected ice just down to the gap layer, however for one core (DC_SL_2) some of the ice below the gap was accidentally collected.

S1.2 M Lead

The M lead, named for the nearby Met City ('MET' on Figure S1 Shupe et al., 2022) separated Met City from the Leg 2 Remote Sensing site (see Nicolaus et al., 2022). We collected 8 cores across the entire width of M lead with a spacing of 1 m on 18 April at approximately 84.48°N, 13.95°E. We sectioned a core from the center of the transect (DC_M_5) and the core closest to the Met City side (DC_M_1). All other cores were collected as bulk samples.

S1.3 T Lead

The T lead (named for the 'Southern' snow and ice thickness Transect) opened on 4 April across the Snow1 sampling area, the S Transect, and adjacent to the Stakes3 mass balance site (Figure S1; Nicolaus et al., 2022). During 5–8 April, ice dynamics occurred in the center of the T lead but not where we would subsequently collect samples from. On 15 April at approximately 84.32°N, 13.77°E, we collected 14 ice cores from two transects in the downwind half of the T lead. The T lead was approximately 20 m wide and was split in the middle by a crack running parallel to the lead that opened the morning we sampled. One transect was perpendicular to the lead and extended 10 m from the downwind edge to the crack (sample spacing 1 m). The other transect ran for 10 m parallel to the lead and was approximately 5 m from the downwind edge. The transects intersected in the middle, and the ice core at this site (DC_T_17) was sectioned. All other cores were collected as bulk samples. Unfortunately, we were unable to access the ice on the upwind half of the lead on 15 April and this ice ridged in the following days.

S1.4 A Lead

The A lead opened on 19 April along the edge of the Snow2 sampling area (Figure S1; Nicolaus et al., 2022) during a warm air intrusion that caused. Most of the leads from 19–20 April ridged and rafted on 21–22 April. However a 6x100 m section of A lead that we would subsequently sample was protected from the ice dynamics by two second-year-ice floes. On 24 April at approximately 84.03°N, 15.87°E, we collected 6 ice cores in a transect across A lead with 1 m spacing. We sectioned a core in the middle (DC_A_3) and all other cores were collected as bulk samples. The core on the side closest to Polarstern (DC_A_6) was noticeably softer than the other cores (i.e. a snow ruler easily went through to the ocean). For all cores, there was not a clear distinction between snow and ice. Although the uppermost 5 cm were softer than below, it appeared that the entire core was composed of the same material. When we revisited A lead on 28 April at approximately 84.03°N, 16.65°E, we collected and sectioned a single core (DC_A_7) from the center of A lead one meter away from DC_A_3.

S2. δ^{18}O of Snow-Free Ice and Snow

Two lines of evidence suggest that most or all of the blowing snow available to be deposited in leads during the A Lead event was from concurrent or very recent precipitation. First, on 16 April (three days prior to the A Lead event) air temperatures warmed up to near freezing, which created patchy glaze crusts and a sintered, hard-to-erode snow surface. Second, as mentioned in the main text, there were three stations that observed the snow surface height with sonic rangers (1 min avg of 1 Hz sampling) positioned over level ice within 1 km of Polarstern—near Met City ('MET' on Figure S1), Balloon Town ('BT' on Figure S1), and BGC1 (Figure S1). These stations did not observe any erosion of the snow that pre-dated 19 April, but they observed 100% erosion of snow that was deposited during 19–21 April. This indicates that it was new snow, not eroded old snow, that was blowing during the event. We identified two surface snow samples that were deposited during the A lead event. One came from a snow drift on 'David's Ridge' (Figure S1) and the other was a snow pit near the Remote Sensing site ('RS' on Figure S1). The δ^{18}O of these snow samples was very similar, -14.4 ‰and -14.2 ‰respectively.

As mentioned in the main text, we use the δ^{18}O measurements from bottom ice samples from the sectioned cores to determine the isotopic composition of snow-free ice (Granskog et al., 2017). Unfortunately, a number of the subsamples were damaged during transit and had to be excluded. Thus we have fewer bottom ice samples (Table S1) than intended, especially for the SL lead (only one sample was usable out of the five that we collected). The δ^{18}O of each usable bottom ice sample was within the measurement uncertainty of all other samples (Figure S2b; note that the error bars are all overlapping). Given this overlap, and that the ice was formed from the same seawater at approximately the same temperature, it is likely that the isotopic composition of snow-free ice for the SL, M, and T leads is essentially the same and most of the variation in mean values (Table S1) is due to measurement noise. For this reason, we combined all bottom ice samples to estimate the distribution of δ_{ref} used for all leads in the main text (the line labelled 'All' in Table S1). To investigate the sensitivity of our results to this choice, we repeated the analysis of snow loss into each lead with δ_{ref} estimated from just the bottom ice samples of that lead (Table S2). The only notable difference is that for the SL lead using δ_{ref} from its bottom ice sample yields a mean snow loss of 1.2 cm instead of 2.2 cm SWE. Note that if this were the case it would actually reinforce the key finding that little snow is lost under typical wintertime conditions. For the A lead, the entire cores were granular, thus there are no bottom ice samples. In the main text we use the same δ_{ref} as the other leads. To test the sensitivity of this assumption, we repeated the analysis for the A lead with δ_{ref} prescribed to be 0.0 ‰(as has been previously assumed: e.g., Jeffries et al., 1997). This assumption would slightly reduce the snow loss into the A lead (Table S2), but does not change the key findings of this work.

References

Clemens-Sewall, D., Macfarlane, A., Fons, S., Granskog, M., Hutchings, J., & Schmale, J. (2022). Salinity and Stable Water Isotopes for Ice Cores in Leads during Leg 3 of the Multidisciplinary drifting Observatory for the Study of Arctic Climate 2020. *Arctic Data Center*. Retrieved 2023-01-08, from `https://arcticdata.io/catalog/view/doi%3A10.18739%2FA23N20G15` (Publisher: Arctic Data Center) doi: 10.18739/A23N20G15

Granskog, M. A., Rösel, A., Dodd, P. A., Divine, D., Gerland, S., Martma, T., & Leng, M. J. (2017, March). Snow contribution to first-year and second-year Arctic sea ice mass balance north of Svalbard. *Journal of Geophysical Research: Oceans*, 2539–

2549. Retrieved 2018-09-26, from https://agupubs.onlinelibrary.wiley.com/doi/abs/10.1002/2016JC012398%4010.1002/%28ISSN%292169-9291.NICE1 doi: 10.1002/2016JC012398@10.1002/(ISSN)2169-9291.NICE1

Hutter, N., Hendricks, S., Jutila, A., Ricker, R., von Albedyll, L., Birnbaum, G., & Haas, C. (2021, July). *Gridded airborne laserscanner (ALS) elevation data (L4) for three flights during MOSAiC (prerelease).* Zenodo. Retrieved 2022-08-19, from https://zenodo.org/record/5121823 (Version Number: 1.0.0-alpha Type: dataset) doi: 10.5281/ZENODO.5121823

Jeffries, M. O., Morris, K., Weeks, W. F., & Worby, A. P. (1997). Seasonal variations in the properties and structural composition of sea ice and snow cover in the Bellingshausen and Amundsen Seas, Antarctica. *Journal of Glaciology*, *43*(143), 138–151. Retrieved 2022-06-19, from https://www.cambridge.org/core/journals/journal-of-glaciology/article/seasonal-variations-in-the-properties-and-structural-composition-of-sea-ice-and-snow-cover-in-the-bellingshausen-and-amundsen-seas-antarctica/D4475C2D538E87C677BB94FCDA38AF06 (Publisher: Cambridge University Press) doi: 10.3189/S0022143000002902

Nicolaus, M., Perovich, D. K., Spreen, G., Granskog, M. A., von Albedyll, L., Angelopoulos, M., ... Wendisch, M. (2022, February). Overview of the MOSAiC expedition: Snow and sea ice. *Elementa: Science of the Anthropocene*, *10*(1), 000046. Retrieved 2022-02-07, from https://doi.org/10.1525/elementa.2021.000046 doi: 10.1525/elementa.2021.000046

Shupe, M. D., Rex, M., Blomquist, B., Persson, P. O. G., Schmale, J., Uttal, T., ... Yue, F. (2022, February). Overview of the MOSAiC expedition: Atmosphere. *Elementa: Science of the Anthropocene*, *10*(1), 00060. Retrieved 2022-06-19, from `https://doi.org/10.1525/elementa.2021.00060` doi: 10.1525/elementa.2021.00060

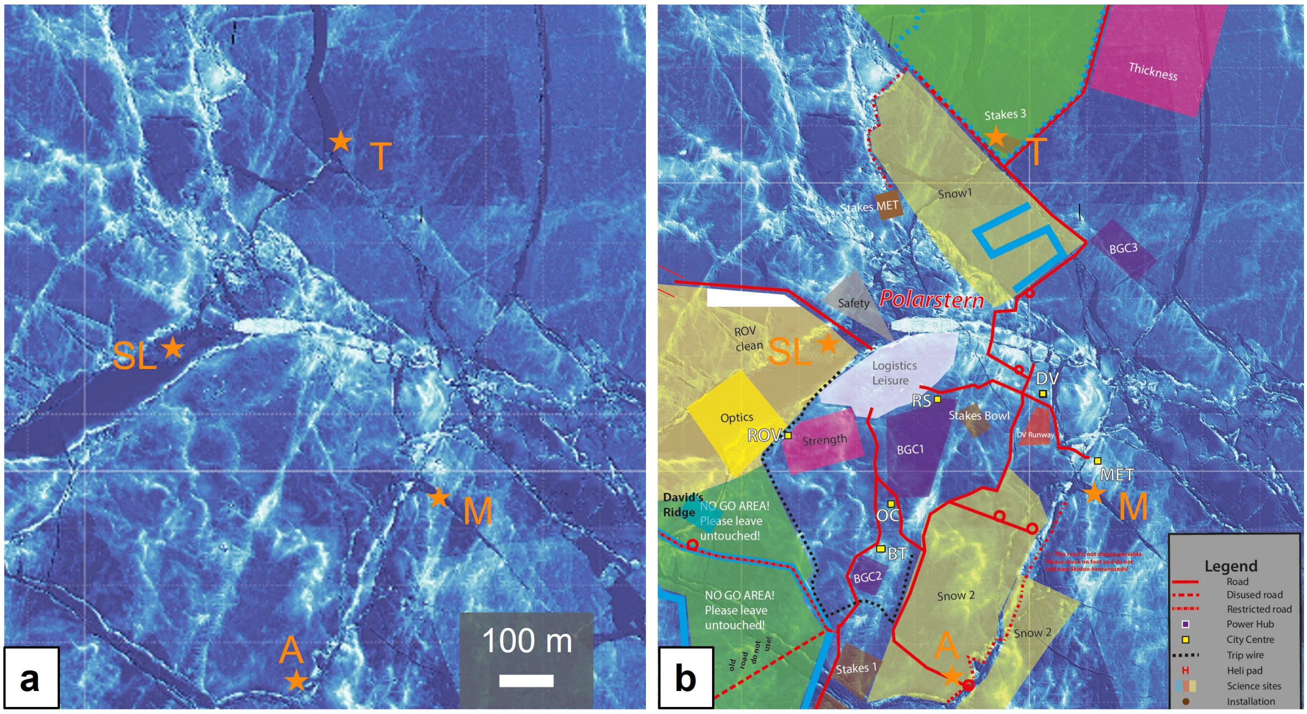

Figure S1. Map of the MOSAiC field site with lead locations indicated by orange stars and labels. The underlying topographic basemap is derived from Airborne Laser Scanning data collected on 8 April 2020 (Hutter et al., 2021). The basemap has been hillshaded such that high areas (e.g., pressure ridges, Polarstern) are white and lower areas are blue. Lead locations are shown on just the topography (a) and on an operational map of the roads and research sites used during the expedition (b). Note that the topography data was collected before the A lead formed. Hence it is not present in the basemap. Thank you to Robert Ricker and Manuel Ernst for processing these data and creating maps respectively while onboard.

Table S1. Parameters for δ_{ref}

Lead	# Bottom ice samples	μ_{ref} (‰)	τ_{ref} (‰)
All	11	2.24	0.15
SL	1	1.81	0.50
M	7	2.17	0.19
T	3	2.54	0.29

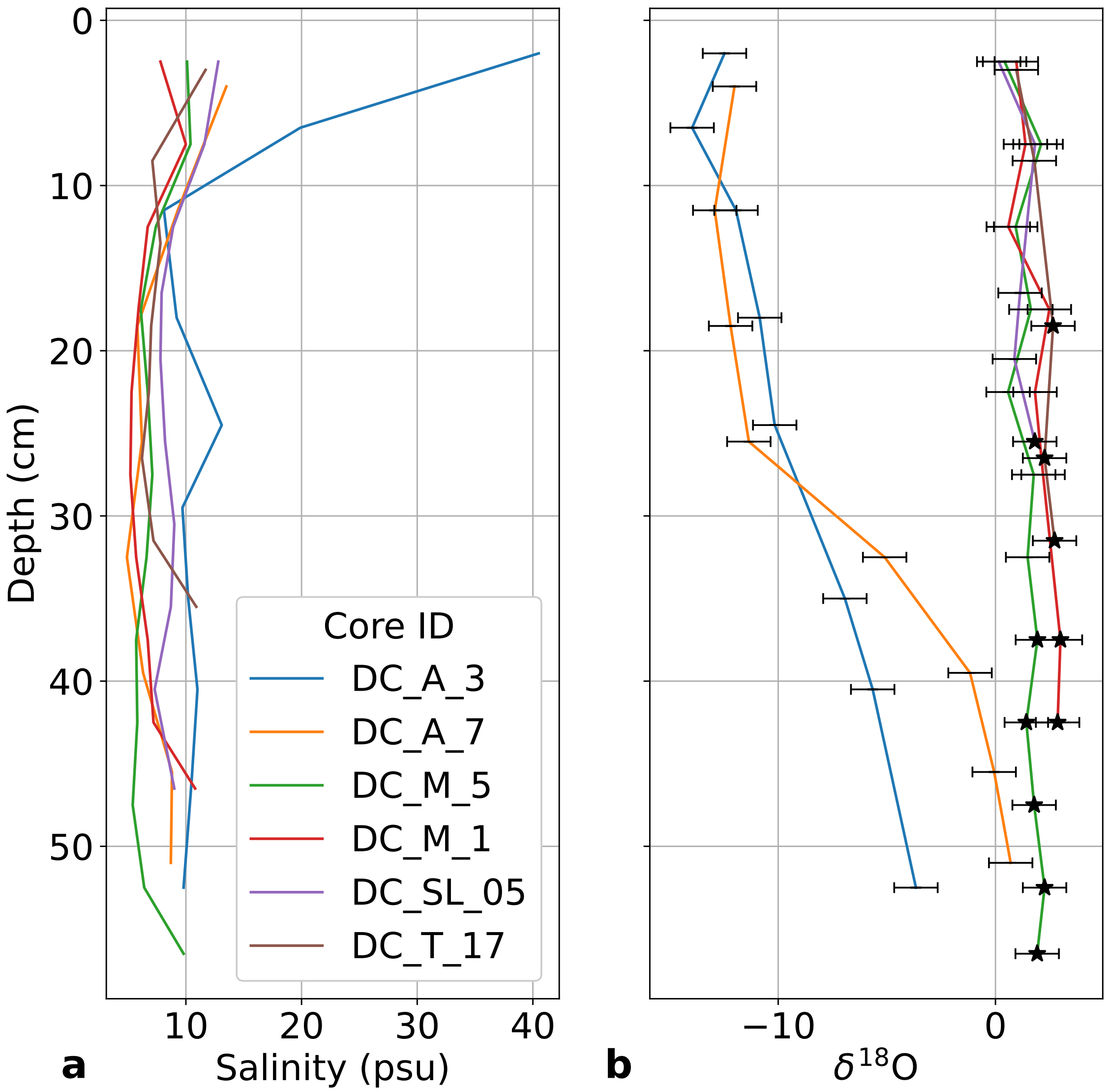

Figure S2. Salinity (a) and δ^{18}O (b) profiles for the sectioned cores. The 'Core ID' for each core includes the lead which it came from (e.g., 'DC_A_3' was the third core in the A lead). The measurement uncertainty at the 95% confidence level in displayed in the horizontal error bars in (b). In (b) samples classified as 'bottom ice' (below the lowermost granular layer) are marked with black stars. Note, if the δ^{18}O subsample was damaged and unusable, we do not display it in (b). This means that in some profiles at some depths we have salinity data (a) but not δ^{18}O data.

Table S2. Snow Loss with Different Assumptions for δ_{ref}

Lead	δ_{ref} Source	Mean SWE (cm)	95% credible interval (cm)
SL	All	2.2	[1.5, 3.0]
	SL	1.2	[0.4, 2.0]
M	All	0.6	[0.1, 1.2]
	M	0.5	[0.0, 1.1]
T	All	0.1	[0.0, 0.4]
	T	0.3	[0.0, 0.7]
A	All	35.0	[33.9, 36.1]
	0[a]	32.4	[31.2, 33.6]

[a] As described in Section S2, this line is if we assume that $\delta_{ref} = 0$ ‰for the A lead.